**Mariusz MĄCZKA[1], Stanisław PAWŁOWSKI[2]**

Politechnika Rzeszowska, Katedra Podstaw Elektroniki (1), Katedra Elektrodynamiki i Układów Elektromaszynowych (2)

# Wannier function applied to quantum cascade lasers modelling

*Abstract. The presented paper deals with one of processes of modeling Quantum Cascade Lasers from the moment the permitted energy bands are determined to specifying Hamiltonian for the device. In the modeling process Wannier quantum states based on Bloch functions are applied. An approach to calculate Wannier functions and numerical results illustrating their fundamental properties, as well as their application to determine Hamiltonian for the laser structure are presented.*

*Streszczenie. Prezentowana praca opisuje jeden ze sposobów modelowania Kwantowych Laserów Kaskadowych od momentu wyznaczania energetycznych pasm dozwolonych do określenia Hamiltonianu przyrządu. W procesie modelowania wykorzystywane są kwantowe stany Wanniera skonstruowane na bazie funkcji Blocha. W ramach artykułu zaprezentowano sposób obliczania funkcji Wanniera oraz wyniki numeryczne ilustrujące ich podstawowe właściwości i zastosowanie podczas określania Hamiltonianu struktury lasera.(**Zastosowanie funkcji Wanniera w procesie modelowania kwantowych laserów kaskadowych**)*

**Keywords**: Quantum Cascade Laser, Wannier functions, Bloch functions.
**Słowa kluczowe**: Kwantowe Lasery Kaskadowe. Funkcje Wanniera, Funkcje Blocha.

### Introduction

Semiconductor devices that emit a coherent light beam within the regions from medium to far infrared are called Quantum Cascade Lasers. Though scientifically recognized for a mere dozen of years [1][2], they have been widely applied in medicine and mining.

From researchers' perspective cascade lasers are low dimension devices, where quantum phenomena play the major role. Therefore, it takes a complex and expensive process to fabricate them, where fine correlation between the material parameters and the expected performance effects is required. Simulations provide a powerful tool to achieve it by properly designing structural design and laser parameters, which contributes to lowering engineering costs.

One of the modeling aspects in such lasers is presented in this paper. A cascade laser simulator comprises many elements, each of them reflecting either the laser structure, or a quantum process occurring in operation. A modular periodic structure, so called semiconducting superlattice (Fig.1), is the main structural element of this device. The modules comprise layers of varying thickness of two semiconductors or their alloys laid alternately. Such interlayered arrangement generates a varying electric potential, which implicitly results in varying probability of finding electrons occupying particular layers. As the quantum mechanics laws hold there, energy bands in such materials split into a number of discrete minibands.
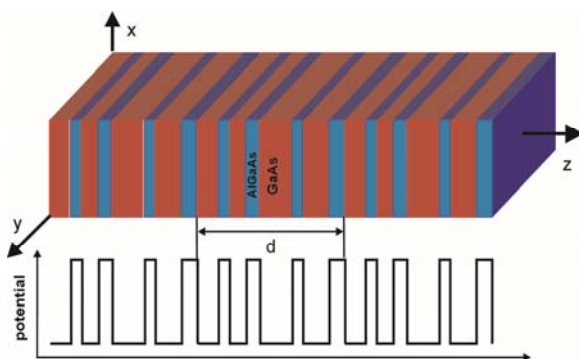


Fig.1. A fragment of semiconductor superlattice structured with AlGaAs layers and GaAs with a depictured $d$-periodic potential produced within the material due to modular semiconductor layers arrangement.

A standard cascade laser structure within one period can be divided into two regions (see Fig.2), namely the active and the injection one.
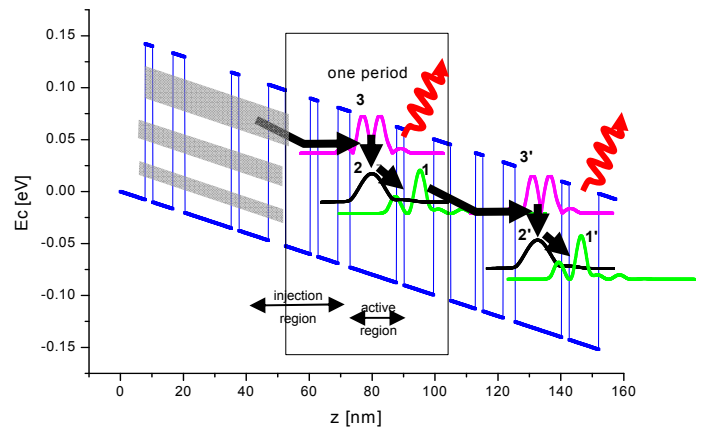


Fig. 2. The fundamental principle of quantum cascade laser operation. The electrons tunnel from the injection region to the upper state (3) of the superlattice next period, which is followed by a transition into a lower state (2) and a photon emission. In the next stage the electron undergoes a transition onto the lowest state (1) accompanied with a phonon emission, then it is transported further by the electric field through the injection region into the higher state of the next structural period (3'), where the whole sequence of transitions between the states is repeated.

In the active region, which comprises one or few quantum wells, three energy states can be recognized, namely the upper (3), the lower (2) and the ground one (1). The electron undergoes transition from the upper level onto the lower one, tunneling at the same time to the next well. It is a radiative transition, thus accompanied with photon emission of energy equal to the difference in the energy between the subbands. Then, the carrier undergoes a transition to the ground level of the well, this time the transition is radiationless, and its energy is absorbed by the lattice in a form of a phonon. It is for the injection region to absorb the electron from the active region ground state and to made it injected onto the upper state (3') of the next active region. It means that one electron provides the source of many photons, thus such lasers are characterized with high output power.

Modeling a quantum cascade laser implies numerical methods to be implemented that allow to determine quantum states and describe the phenomena related to transport of charge carriers located in a periodical potential. Under a joined PR-ITE research project a simulation method based on the nonequilibrium Green function theory [3] operating within the real space base was developed. Yet, the proposed approach requires substantial processor

capacities, and vast operational storage resources for the computers dedicated to such calculations, thus a more efficient method is under concurrent development [4]. The latter operates within the state space base, exploiting non-equilibrium Green functions. Wannier functions play a significant role in this method [5], as they provide for the very structural element of the energy states occurring in both photon and phonon emission processes.

A process for constructing Wannier states, and the way they are used while simulating a typical quantum cascade laser [6] are also presented in this paper.

## Model for cascade laser structure

The presented paper deals with a non-symmetrical superlattice of a semiconductor layer structure arrangement typically applied in technological solutions for quantum cascade lasers. The fundamental material is composed of two GaAs/Al$_{0.15}$Ga$_{0.85}$As layers laid interchangeably, which forms a superlattice module. Specific layers thickness in nm are 7.8/2.4/6.4/3.8/14.8/2.4/9.4/5, respectively. Such a structure was fabricated and reported by Hans Callebaut in 2005 [6].

A numerical model for the structure referred to above, is presented in Figure 3. It is composed of n modules of d length each, comprising the layer arrangement explained above, which produces a periodic potential modeling the bottom conduction band $E_C$ – in structure, where difference in values between the quantum well bottom and the energetic barrier height equals $\Delta E_C$=150 meV. Under thermodynamic equilibrium within a semiconductor single layer ($z_j<z<z_j+1$) a constant potential $V_j$ and a uniform composition of material represented with electron effective mass parameter $m_j$ were assumed.
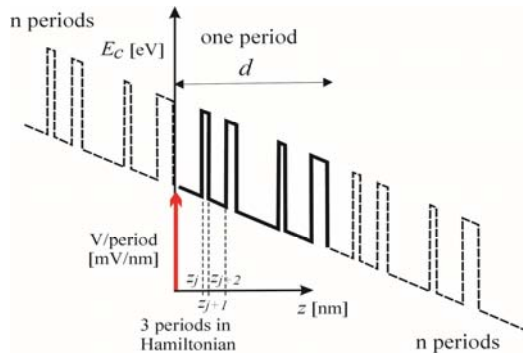


Fig. 3. A structural model for a cascade laser fabricated on GaAs/Al$_{0.15}$Ga$_{0.85}$As superlattice base. The illustrated case represents thermodynamic non-equilibrium. The model comprised an infinite number n of $d$ length modules, each composed of the layer arrangement decoded in nanometers as 7.8/**2.4**/6.4/**3.8**/14.8/**2.4**/9.4/5, where Al$_{0.15}$Ga$_{0.85}$As regions are marked in bold. Such conducting layers produce a periodic potential, which models the energy scheme of the bottom of the material conduction band - $E_c$ with the difference in values between the quantum well bottom and the energetic barrier height $\Delta E_c$=150 meV.

When voltage is applied to the structure under this model it functions as recalculated to one superlattice period. The superlattice model presented in Fig. 3 is an infinite one. Its specific properties have been described elsewhere [4].

## Determining permitted minibands

Permitted energy minibands within the structure of the considered laser have been calculated with one of the numerical methods applied to solving the Schrödinger equation. By this method, called Transfer Matrix Formulation [5] a solution in a form of the following function is sought

(1)     $\psi_j(z) = A_j e^{ik_j(E)(z-z_j)} + B_j e^{-ik_j(E)(z-z_j)}$,

where relation:

(2)     $k_j(E) = \sqrt{2m_{c,j}(E-V_j)}/\hbar$

includes the electron effective mass $m_{c,j}$ and potential $V_j$ for the $j$-th layer of the heterostructure with the following continuity conditions at the region border:

(3)     $\psi_j(z_{j+1}) = \psi_{j+1}(z_{j+1})$

(4)     $\dfrac{1}{m_{c,j}}\dfrac{\partial \psi_j}{\partial z}\bigg|_{z=z_{j+1}} = \dfrac{1}{m_{c,j+1}}\dfrac{\partial \psi_{j+1}}{\partial z}\bigg|_{z=z_{j+1}}$

By the Bloch condition:

(5)     $\varphi_q(z+d) = e^{iqd}\varphi_q(z)$

where $q$ is the Bloch vector component in $z$ axis direction, we obtain a matrix equation:

(6)     $\begin{pmatrix} A_{N+1} \\ B_{N+1} \end{pmatrix} = M \begin{pmatrix} A_1 \\ B_1 \end{pmatrix} = e^{iqd} \begin{pmatrix} A_1 \\ B_1 \end{pmatrix}$

where:

(7)     $M = M_N M_{N-1} ... M_1$

$N$ index denoted the number of layers within a superlattice period, while $M_N$ stands for the transition matrix in the form:

(8)     $M_N = \dfrac{1}{2}\begin{pmatrix} (1+\alpha_j)\cdot e^{ik_j w_j} & (1-\alpha_j)\cdot e^{-ik_j w_j} \\ (1-\alpha_j)\cdot e^{ik_j w_j} & (1+\alpha_j)\cdot e^{-ik_j w_j} \end{pmatrix}$

with $w_j = z_{j+1} - z_j$ and $\alpha_j = \dfrac{k_j m_{c,j+1}}{k_{j+1} m_{c,j}}$

Solving equation (6) allows to determine the permitted energy ranges for the cascade laser structure under consideration, as well as the dispersion relation $E = E(q)$. The results of this part of simulation are presented in Table 1 and in Fig. 4.

Table 1. The permitted minibands ranges calculated with TMF method for the considered cascade laser structure.

| miniband | Energy range [eV] |
|---|---|
| a | 0.0146625 - 0.0146678 |
| b | 0.0290264 - 0.0292115 |
| c | 0.0337528 - 0.0340779 |
| d | 0.0506446 - 0.0511524 |
| e | 0.0619844 - 0.0625063 |

As shown in the Table 1 the value ranges are very narrow for the permitted energy bands, hence they were coined as minibands. In Fig. 4 the results are presented as dependencies of the permitted energies for the five lowest energy minibands on the Bloch vector component in the direction of $z$ axis.

For the purpose of this paper the simulation results the dispersive relations Bloch functions presented in the form (1) are replaced with Bloch states $\varphi_q^v(z)$, derived by applying the dispersion equation denoted as [5]:

(9)     $E^v(q) = E^v + \sum_{h=1}^{\infty} 2T_h^v \cos(hdq)$

Bloch states in their new formulation make the permitted energy $E$ within the miniband $\nu$ dependent on the Bloch vector component ($q$), in the direction where charge carriers are transported, i.e. $z$ axis.
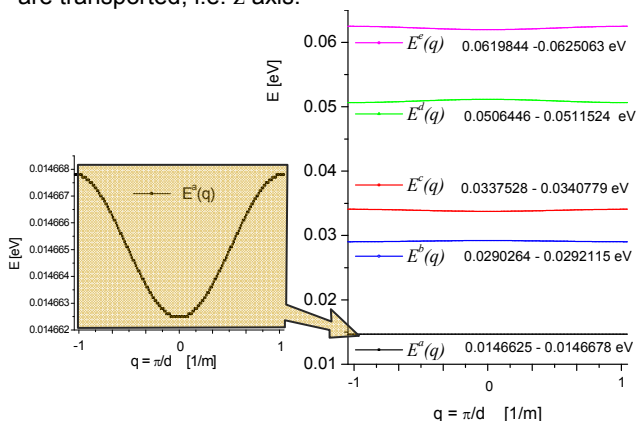


Fig. 4. Permitted energy minibands in the considered cascade laser structure presented as dependent on the Bloch vector $z$ axis component $E^\nu(q)$. The A part shows a blown fragment of $E^a(q)$

According to Kramers degeneration theory it can be noted that $E^\nu(q) = E^\nu(-q)$ and $-\pi/d < q < \pi/d$. The parameter $T_h^\nu$ in equation (9) determines the hopping coefficient between the minibands

**Bloch states and Wannier functions.**
Each energy of a particular miniband corresponds to one Bloch function, whose form within each structure layer is described by (1).
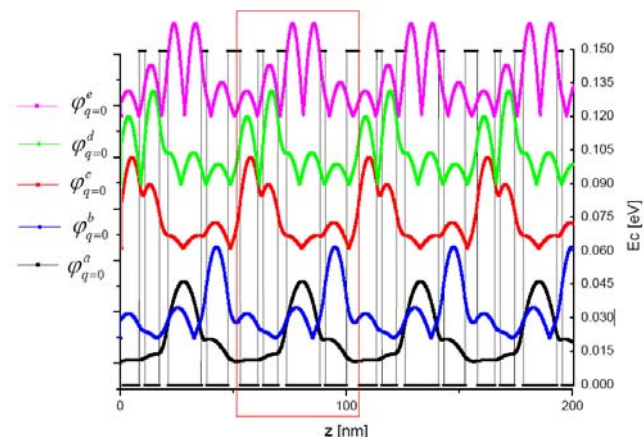


Fig. 5. Module dependencies for the selected Bloch states for the five minibands lowest in the energy domain. The state upper index denotes the miniband, while the lower one reflects the plotted Bloch vector component ($q$). The plotted functions are set against periodic potential generated by the superlattice structure.

Bloch states derived by applying relation (9) are illustrated in Fig. 5. Selected modules of complex Bloch function for $q=0$ within each considered miniband are plotted. The zero component Bloch vector – $q$ denotes the bottom permitted band energy for minibands $a$, $c$, $e$ while the energy of the permitted band node for minibands $b$, $d$.

Periodicity of the 5 states presented in Fig. 5 within the superlattice module is very characteristic; it results from applying an infinite superlattice model complemented with Bloch conditions. It is also easy to note that the lowest states are strongly localized, whereas the higher the state, the weaker localization within the single quantum well occurs. It is related to the width of the quantum wells forming a superlattice module. The widest well localizes

within itself the lowest energy state, while subsequently wider wells localize further higher and higher energy states.

The phases of complex Bloch states are of significant importance for cascade laser simulations within an indefinite model (IM) approach.
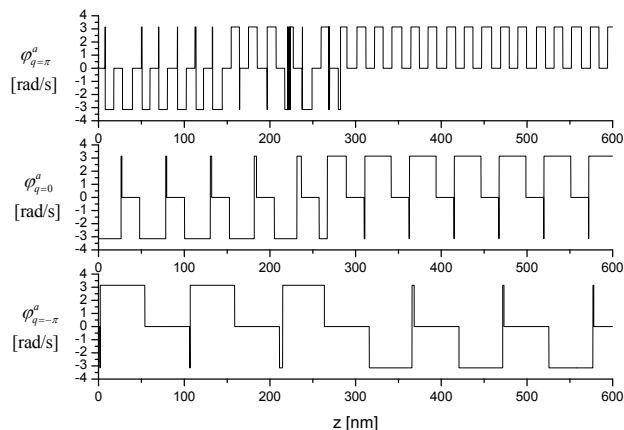


Fig. 6. Phase dependencies for three selected Bloch states for the lowest in the energy domain miniband denoted as $a$. The values for the Bloch vector component $q$ were selected to represent the miniband middle and extreme parts.

Phase dependencies for the selected Bloch states within the first miniband are pictured in Fig. 6. It shows that for the studied laser structure, the complex Bloch functions phases vary irregularly. Still, they are greatly shaped by the places where zero initial phases are assumed. It all shapes the final form quantum states take applied to define the device Hamiltonian; the latter will be discussed further in the paper.

Bloch states obtained by applying equation (9) on the one hand allows the continuous miniband to be discretized with respect to the Bloch vector component and, on the other, facilitates Wannier functions to be calculated in the form [5]:

$$(10) \qquad W^\nu(z - nd) = \sqrt{\frac{d}{2\pi}} \int_{-\pi/d}^{\pi/d} \varphi_q^\nu(z) \cdot e^{-inqd} \, dq$$

Wannier functions, obtained with (10) provide a solution to the Schrödinger equation, alike Bloch functions, but they are not its eigenstates, i.e. they do not correspond to the eigenenergies of the system. Selected dependencies for the modules of the complex Wannier functions for the five minibands lowest in the energy domain are depicted in Fig. 7. It displays non-periodic and non-localised functions obtained on the base of relation (10) with zero values for the Bloch function initial phase set. These are indicated by lower indices of particular Wannier function as parameter values $z_{fo}$.

Wannier functions presented in Figure 7, though relatively easy to calculate, do not have a form suitable for the cascade laser simulation method, as it requires functions to be maximally localized. To obtain such a maximally localized Wannier state the initial phases of the complex Bloch function it is formed with, shall be selected to generate maximum values of the real part, preferably within one quantum well and one superlattice period.

Then, the imaginary part of the Wannier state values practically equal zero over the entire state. Under the presented research the maximum localisation for each state was attained by applying numerical procedures that analysed both real and imaginary values of Wannier function, as well as the values of the integral enveloped by them for various initial phase values of Bloch functions they are generated by.
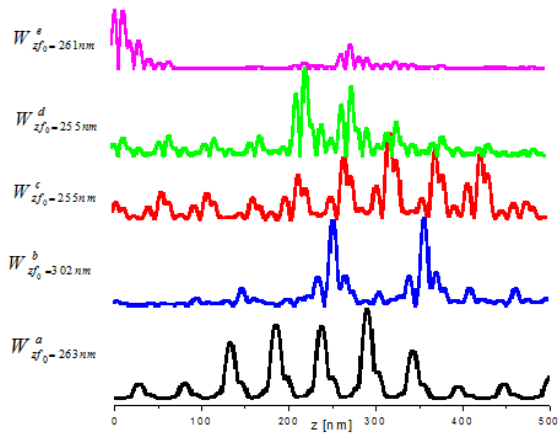
Fig. 7. Dependencies of modules for the selected Wannier functions for the five minibands lowest in the energy domain. The upper index of the particular function denotes the miniband code, whereas the lower one corresponds to zero value of the complex Bloch states initial phase.
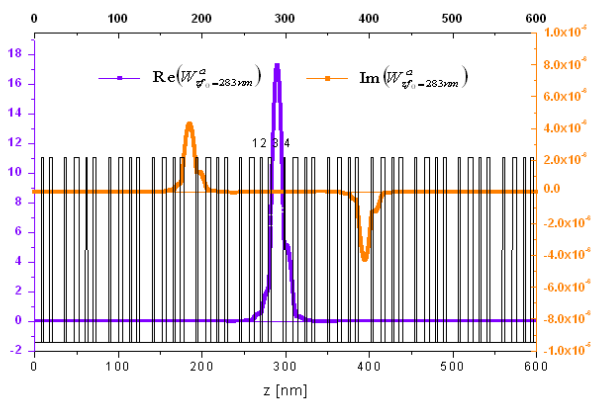


Fig. 8. Dependencies of the real ($\mathrm{Re}(W^a_{zf_0=283nm})$) and imaginary ($\mathrm{Im}(W^a_{zf_0=283nm})$) parts for the maximally localised Wannier functions for the first miniband denoted as $a$. The values for $z_{fo}$ variable given in the function lower index indicates where the Bloch states initial phase become zero. In order to correlate the function dependence within the laser structure better, it is set against the superlattice periodic potential with numbers 1 to 4 marking the subsequent quantum wells comprised within one superlattice module

In Fig. 8 the real part ($\mathrm{Re}(W^a_{zf_0=283nm})$) and imaginary ($\mathrm{Im}(W^a_{zf_0=283nm})$) part of maximally localised Wannier functions for the first miniband, denoted in this paper as a, are plotted. It can be observed that, as signalled before, for the maximal localisation of Wannier function it is necessary for its real part to reach the maximum values within a specific quantum well, represented here with well 3, and for its real part to be minimised to nearly zero values at the same time. Analysing Wannier functions with respect to this angle while applying numerical procedures, lead us to the results illustrated in Fig. 9, where the squared modules of the maximally localized Wannier functions for all the minibands dealt with in this paper are plotted. Our results confirm results reported elsewhere [7].

By comparing functions plotted in Fig. 7 and 9 the following conclusions can be drawn. Firstly, Wannier functions are very sensitive to spatial setting null values for Bloch states initial phases in the course of their integration (see formula (10)), and secondly, the fact that Wannier functions is maximally localised does not correlate with any

rule on Bloch states initial phase taking zero value. It is much evident for the quantum state of the miniband denoted as $b$, which finally localises in the quantum well no 4 with Bloch function initial phase zero value set at 304 nm. Nevertheless, it is enough to shift the null valued of the Bloch function initial phase by 2 nm to the left to the value of 302 nm (se Fig. 7), for the very state to become clearly delocalised. Therefore, it proves not that easy to obtain maximally localised Wannier states and it requires further numerical research to be performed.
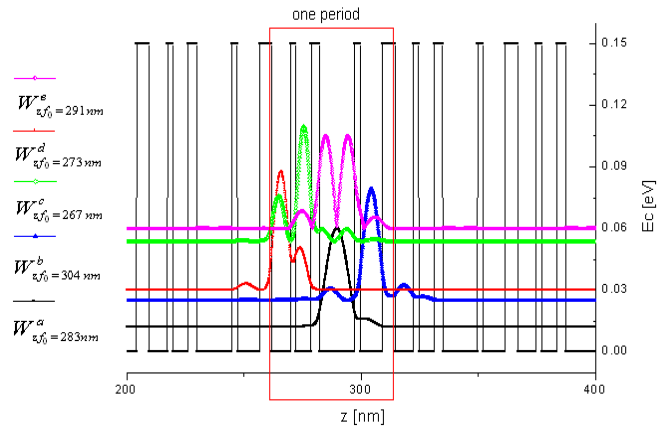


Fig. 9. Dependencies of the squared modules of maximally localised Wannier functions for the five minibands lowest in the energy domain. The function upper index gives miniband notation, whereas the lower one corresponds to the zero value for the complex Bloch state initial phase.

### Cascade Laser Hamiltonian

Maximally localised Wannier states are requisite to determine a Hamiltonian for the electron in a cascade laser. Such a Hamiltonian may take the form of :

$$(11) \qquad \hat{H} = \hat{H}_{SL} + \hat{H}_{\xi} + \hat{H}_{scatt}$$

where $\hat{H}_{SL}$ stands for the structure Hamiltonian disregarding the field, $\hat{H}_{\xi}$ stands for a Hamiltonian where electric field was taken into account, whereas $\hat{H}_{scatt}$ concerns also inelastic electron scattering. Wannier states are applied to form the Hamilton matrix for the second and third addend of (11). This paper deals with applying these states to the process of constructing the Hamiltonian matrix where electric field has been taken into account, and which can be written as:

$$(12) \qquad \mathbf{H}_{\xi} = \sum_{n,\nu} \sum_{\mathbf{k}} \left\{ \begin{array}{l} -e\xi R_0^{\mu\nu} \hat{a}_{n,\mathbf{k}}^{\nu\dagger} \hat{a}_{n,\mathbf{k}}^{\nu} - ne\xi d\delta_{\mu\nu} \hat{a}_{n,\mathbf{k}}^{\nu\dagger} \hat{a}_{n,\mathbf{k}}^{\nu} - \\ + e\xi R_1^{\mu\nu} \left[ \hat{a}_{n+1,\mathbf{k}}^{\nu\dagger} \hat{a}_{n,\mathbf{k}}^{\nu} + \hat{a}_{n-1,\mathbf{k}}^{\nu\dagger} \hat{a}_{n,\mathbf{k}}^{\nu} \right] \end{array} \right\}$$

where $e$ stands for electron charge, $\xi$ denotes electric field intensity, n corresponds to the number of the superlattice period concerned, whose length is represented with variable $d$, $\mathbf{k}$ stands for wave vector, while $\hat{a}_{n,\mathbf{k}}^{\nu\dagger}$ and $\hat{a}_{n,\mathbf{k}}^{\nu}$ parameters are state operators of creation and annihilation, respectively. The quantity $R_l^{\mu\nu}$ is calculated from the relation:

$$(13) \qquad R_l^{\mu\nu} = \int dz\, W^{\mu*}(z-ld) z W^{\nu}(z)$$

called state overlap integral. This relation allows both for permitted interstate interaction (indexes $\mu,\ \nu$) and for

superlattice period (index $l$). The values the overlap integrals assume for the maximally localised Wannier states are given in Tables 2 and 3.

Table 2. The overlap integrals values $R_l^{\mu\nu}$ calculated with relation (12) for the parameter $l=0$, i.e. interactions within the same superlattice period.

| $\mu$ \ $\nu$ | 1 | 2 | 3 | 4 | 5 |
|---|---|---|---|---|---|
| 1 | (2.907e-7, 1.061e-37) | (1.863e-8, -5.587e-16) | (4.643e-9, -1.113e-17) | (-5.556e-10, -2.797e-18) | (1.312e-8, -9.978e-15) |
| 2 | (1.863e-8, 5.587e-16) | (3.035e-7, 2.238e-31) | (2.742e-9, -7.513e-15) | (3.325e-9, 1.348e-16) | (2.834e-9, 1.039e-14) |
| 3 | (4.643e-9, 1.113e-17) | (2.742e-9, 7.513e-15) | (2.676e-7, 9.958e-34) | (6.570e-9, 1.482e-17) | (1.396e-8, 2.989e-14) |
| 4 | (-5.556e-10, 2.797e-18) | (3.325e-9, -1.342e-16) | (6.570e-9, -1.482e-17) | (2.747e-7, -3.311e-33) | (-3.239e-8, 1.242e-12) |
| 5 | (1.312e-8, 9.978e-15) | (2.834e-9, -1.039e-14) | (1.392e-8, -2.989e-14) | (-3.239e-8, -1.242e-12) | (2.896e-7, -7.264e-30) |

Table 3. The overlap integrals values $R_l^{\mu\nu}$ calculated with relation (12) for the parameter $l=1$, i.e. interactions within the adjacent superlattice periods.

| $\mu$ \ $\nu$ | 1 | 2 | 3 | 4 | 5 |
|---|---|---|---|---|---|
| 1 | (-2.84e-10, -3.245e-16) | (1.23e-9, -9.345e-15) | (1.346e-10, 1.108e-16) | (-8.96e-11, -4.272e-18) | (1.474e-9, -4.609e-14) |
| 2 | (1.874e-10, -3.637e-14) | (4.529e-9, -5.168e-13) | (1.664e-10, -8.118e-14) | (1.731e-10, -3.639e-15) | (-2.529e-10, -1.344e-13) |
| 3 | (-2.021e-9, 2.004e-18) | (3.979e-9, -3.463e-16) | (3.751e-9, 5.182e-15) | (-8.05e-10, 5.393e-17) | (-6.678e-9, -1.248e-13) |
| 4 | (3.927e-10, 2.298e-17) | (3.885e-11, -4.679e-15) | (-8.360e-11, 8.758e-17) | (5.234e-9, -4.759e-17) | (3.213e-9, -7.297e-12) |
| 5 | (2.746e-12, 9.556e-15) | (2.231e-9, -1.149e-14) | (3.118e-10,-2.958e-14) | (-2.372e-9, -1.241e-12) | (-4.854e-9, 7.030e-13) |

By analysing the numerical results presented in Tables 2 and 3 it can be concluded that restricting quantum states interactions to the adjacent superlattice periods seems reasonable as we can see from the equation $R_0^{11}$ (2.907e-7 + i 1.061e-37) and $R_1^{11}$ (-2.848e-10 – i 3.245e-16) the overlap integrals for the adjacent periods ($l=1$) are diminished by circa 4 orders of magnitude, when compared to the basic period ($l=0$). Therefore, neglecting the interactions between the superlattice periods farther than the adjacent ones, does not significantly influence laser operation simulation results, whereas it significantly accelerates calculations. It should be stressed, however, that for this situation to take place the quantum states used for Hamiltonian must be maximally localised.

**Summary**

Under presented research software modules for simulating cascade lasers based on the method exploiting Wannier functions properties were successfully developed and tested. Applying Wannier functions allowed the Hamiltonian for the concerned nanodevice to be written as an energetic representation, due to the fact that the size of the matrix representing this operator is small. With properly calculated maximally localised Wannier functions it is enough for the simulation process to take into account only the interactions between the quantum states of the adjacent superlattice periods, which allows the size of the matrix representing the total Hamiltonian for the laser to grow insignificantly, thus the simulator is effective.

REFERENCES

[1] Faist J., Capasso F., Sivco D. L., Sirtori C., Quantum Cascade Laser, *Science*. 264. 5158, s. 553 – 556, 1994.
[2] Kosiel K., Bugajski M, Szerling A, Kubacka-Traczyk J, 77 K operation of AlGaAs/GaAs quantum cascade laser at 9 um., *Photonics Letters of Poland*. 1. 1, s. 16-18, 2009.
[3] Hałdaś G., Kolek A., and Tralle I., Modeling of Mid-Infrared Quantum Cascade Laser by Means of Nonequilibrium Green's Functions, *Journal of Quantum Electronics*, vol. 47, no. 6, JUNE 2011.
[4] Mączka M., Pawłowski S., Plewako J. Comparative analysis of selected models of semiconductor superlattices, *Electrical Review*, 8/2011, p.p. 93.
[5] Wacker A., Semiconductor superlattices: a model system for nonlinear transport, *Physics Reports*, vol. 357 (2002), pp. 1-111.
[6] Callebaut H. and Hu Q., *J. Appl. Phys*. 98, 104505 (2005).
[7] Lee S.-C., Banit F., Woerner M., and Wacker A., Quantum-mechanical wavepacket transport in quantum cascade laser structures. *Physical Review B*, vol. 73, 245320 (2006).

*Authors*: dr inż. Mariusz Mączka, Politechnika Rzeszowska, Katedra Podstaw Elektroniki, ul. W. Pola 2a, 35-959 Rzeszów, E-mail: mmaczka@prz.edu.pl; prof. dr hab. inż. Stanisław Pawłowski, Politechnika Rzeszowska, Katedra Elektrodynamiki i Układów Elektromaszynowych E-mail: spawlo@prz.edu.pl.